Turkish Journal of Engineering

Turkish Journal of Engineering (TUJE)
Vol. 3, Issue 2, pp. 76-91, April 2019
ISSN 2587-1366, Turkey
DOI: 10.31127/tuje.454978
Research Article

REGIONAL GEOELECTRICAL DIMENSIONALITY OF THE NORTHWESTERN PART OF TURKEY FROM MAGNETOTELLURIC TENSOR INVARIANTS

Fahriye Akar [*1] and Cemal Kaya [2]

[1] Erzincan University, Department of Construction Technologies, Erzincan, Turkey,
ORCID ID 0000-0002-8445-0353
fhrykcmzb@gmail.com

[2] Kayaç Yer Bilimleri, Private Company (Owner), Ankara, Turkey,
ORCID ID 0000-0002-1065-0205
cemal.kaya2010@hotmail.com

* Corresponding Author
Received: 23/08/2018 Accepted: 15/09/2018

ABSTRACT
In this study, measurements obtained through the first two profiles from the TÜBİTAK (The Scientific and Technological Research Council of Turkey) project titled "Research of the Crustal Structure of Northwestern Anatolia with Geophysical Methods" from 2007 were used. Magnetotelluric (MT) measurements were taken from 174 sites approximately every 3 km in the region between Zonguldak and Akşehir (Konya). Dimensionality analysis was conducted with the decomposition of the impedance tensor obtained through the measurement data from the two profiles. The relationship between the observed geo-electric behaviors, the geological structure of the area and the MT dimensionality changes were detected. Two-dimensional (2D) and three-dimensional (3D) structures were revealed as a result of the dimensionality analysis obtained through the MT data from the region located between Zonguldak and Akşehir. The dimensionality was observed to be complex in small periods due to the heterogeneous conductive materials close to the surface and 3D structures were observed to be predominant in high periods. Moreover, the dimensionality near the suture zones were observed to be more complex compared to other areas according to the dimensionality analysis results. The structures in the vicinity of the North Anatolian Fault were found out to be N-NE striking. This indicates the accuracy and reliability of the results.

Keywords: *Magnetotelluric Method, Geoelectric Dimensionality, Geoelectric Struture, Northwestern Anatolian*

1. INTRODUCTION

The MT data could be interpreted 1-, 2- or 3-dimensionally with the dimensionality analysis. Usually, the constants found through the decomposition of the tensor components obtained from the MT data measured at the site are used for determining the dimensionality. Distortions and strike directions of geo-electric structures can also be found via dimensionality analysis. MT data are affected by distortions that mask the dimensionality of earth electricity structures and this may lead to wrong interpretations. For the correct interpretation of the data in magnetotelluric method, distortions should be defined and kept away from the data. Therefore, a good dimensional analysis is necessary.

Dimensionality analysis is a significant part of the MT study. There are several methods used to determine the dimensionality of the underground structures and they are usually based on rotational invariants. Swift (1967), Berdichevsky and Dimitriev (1976), Bahr (1988), Bahr (1991), Lilley (1993, 1998a, 1998b) made classifications of dimensionality using groups of parameters calculated via the measured MT tensors. Ranganayaki (1984), Ingham (1988), Park and Livelybrooks (1989) revealed 1D structures using the impedance average. Swift (1967) researched whether structures were 2D or not by using MT data. Bahr (1988) researched whether the 3D structures and measured MT data were affected from distortions caused by small local anomalies or not. Fischer and Masero (1994) suggested 7 independent and 1 dependent invariables using the components defining impedance tensor. Szarka and Menvielle (1997) formed a group of MT tensor invariants to be used in dimensionality analysis by thoroughly examining the rotational features of MT tensor. Romo *et al*. (1999) used invariant parameters obtained through magnetic transfer function (tipper) to define 2D and 3D reactions. Weaver et al. (2000) made a definition of geoelectric dimensionality using the rotational invariants they obtained from the MT tensor. Caldwell et al. (2004) put forward the notion of MT phase tensor using the relation between the real and virtual parts of the MT tensor. In this study, the dimensionality analysis of the geologically complex region between Zonguldak and Akşehir was carried out with Wal invariants obtained from impedance tensor, using the measurements from 173 MT points (Weaver et al., 2000).

This study aimed at determining the dimensionality of geoelectric structure and strike directions in the study site, contributing to gathering more information on the geology of the site, which has a complex structure.

2. MT DATA ACQUISITION

North to East measurements were taken along the two profiles located in western Turkey in 2007 were used in this study. The first profile passes through Kıbrıscık, Kırbaşı, Beypazarı, Günyüzü, Çeltik, Yunak and Turgut; the second profile passes through Akçakoca, Düzce, Dokurcun Valley, Emirdağ, Bolvadin and Çay (Fig.1). Magnetotelluric (MT) measurements were taken from a total of 174 points, approximately every 3 km along both profiles.

Fourier transforms were applied on the measured time series magnetotelluric data, impedances were obtained in frequency setting and files were created in EDI (Electrical Data Interchange) standards.

Potential electrodes consisting of four nonpolarized conductive ceramic cables containing lead-lead chloride (Pb-$PbCl_2$) were used to measure the electric field.
The distance between electrodes ranges between 50 to 200 m depending on the site conditions. The electrodes in North-South direction are called Ex and the ones in East-West direction are called Ey. Electrodes are placed in approximately 25 cm deep pits filled with mud.

The magnetic field is measured with induction coils that has a conductor in the core. Coils used in this study are sensitive to the range between 400 Hz and 0.00002 Hz. The horizontal coils are placed in parallel with the north-east direction. The coil placed as the free end pointing towards north is called hx and the coil placed as the free end pointing towards east is called hy. The third coil called hz should be placed vertically in a pit deep enough to cover the whole coil, as delicately as possible.

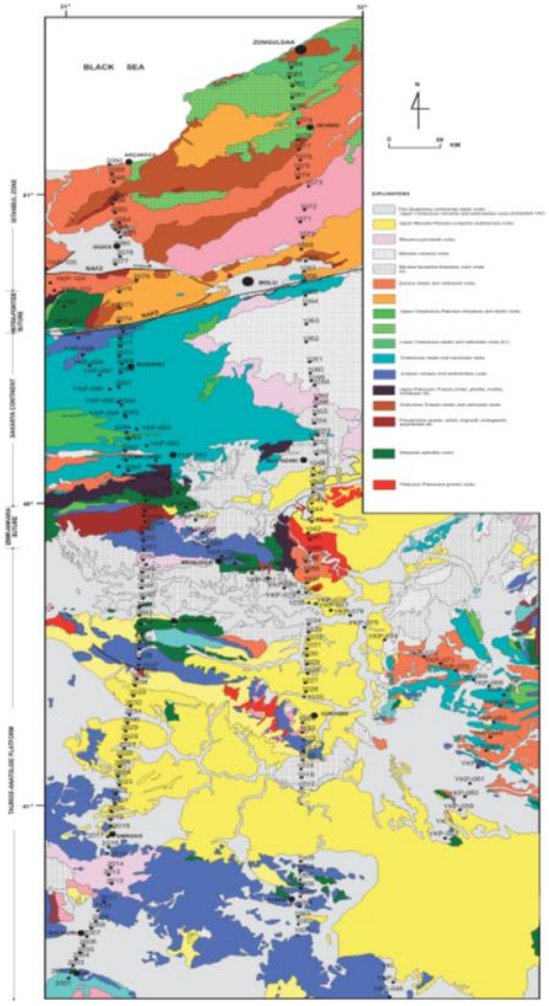

Fig. 1. Geologic map of the study site, drawn based on the 1/500,000 scale Geological Map of Turkey Ankara, Zonguldak map sheets, General Directorate of MTA (Mineral Research and Exploration) 2002.

3. GEOLOGICAL SETTING

It is generally accepted that there are 6 main lithospheric plates in Turkey, namely Istranca, İstanbul and Sakarya zones, Torid-Anatolid Block, Kırşehir Massif and ArabicPlatform (Şengör and Yılmaz 1981; Şengör et al. 1982; Okay 1989; Okay et al. 1994). The main continental pieces and suture zones in and around Turkey are shown in Fig. 2.

The region in the Northwest Anatolia extending from the Black Sea to Araç-Daday-İnebolu is known as the İstanbul Zone (Okay, 1989). Şengör and Yılmaz (1981), Şengör et al. (1984), Tüysüz (1990) stated that the İstanbul Zone was a pre-Dopper nappe; Okay et al. (1995) stated that it settled in its current location after rifting from the Moesian platform in Cretaceous period; Yılmaz et al. (1997) stated that the Sakarya Continent and Istranca Zone united due to Paleotethys and its continuation Intra-Pontide oceans coming together between the end of the Triassic period and the Cretaceous period; and Tüysüz (1999) stated that the east end of the İstanbul Zone was bordered by the Intrapontide Suture.

Intra-Pontide Suture constitutes the border between the İstanbul Zone and Sakarya Continent. Currently, it corresponds to the North Anatolian Fault, which is a post-Miocene strike-slip fault (Okay & Tüysüz, 1999; Okay Güncüoğlu 2004). E-W trending Sakarya Zone located between the Intra-Pontide suture and İzmir-Ankara suture lies along the profiles towards south. Triassic subduction-accumulation units named as the Karakaya Complex include the lower section of the Permo-Triassic metabasite-marble-phyllite series with exotic Triassic lenses of eclogite (Monod et al., 1996; Okay and Monié, 1997).

İzmir – Ankara – Erzincan Suture, which is one of the most important sutures of Anatolia, represents the closing of the north arm of the Tethys Ocean between Laurasia and Gondwana from late Paleozoic to early Tertiary period. It separates the Sakarya Continent from the Anatolide-Tauride Block in north to south direction (Okay and Tüysüz, 1999). Tavşanlı Zone is a subsection of the Anatolide-Tauride Block (Fig. 2). Together with the Neotethyan Ocean, it is a metamorphic arch formed due to the subduction of the northern edge of the Anatolide-Tauride Block (Okay, 1982, 1986; Sherlock et al., 1999; Droop et al., 2005).

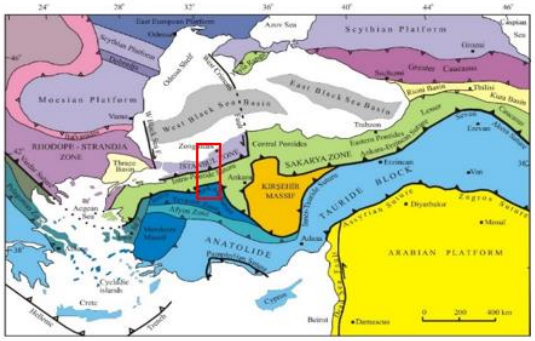

Fig. 2. Tectonic map of the eastern Mediterranean region showing large troops and suture borders. Full triangles indicate dipole polarity, red rectangular shows study area (Okay and Tüysüz, 1999).

MT profiles start from the Tavşanlı Zone, pass through İzmir-Ankara-Erzincan Suture zone, Sakarya zone and the Intra-Pontide suture and end at the İstanbul Zone.

4. WAL DIMENSION ANALYSIS

Weaver et al. (2000) aimed at finding out information about the underground dimensionality by producing rotational invariant parameters (WAL invariants) from the MT tensor. WAL invariant linear combinations of the complex parameters obtained through decomposition of the real and imaginary parts of the MT tensor, which is a complex number, was found with $\zeta_i = \xi_i + \eta_i i$ (i=1,4). These complex parameters are given as follows;

$$\zeta_1 = (M_{xx} + M_{yy})/2, \tag{1}$$

$$\zeta_2 = (M_{xy} + M_{yx})/2, \tag{2}$$

$$\zeta_3 = (M_{xx} - M_{yy})/2, \tag{3}$$

$$\zeta_4 = (M_{xy} - M_{yx})/2 \tag{4}$$

From here, the MT tensor is defined with:

$$M = \begin{pmatrix} \zeta_1+\zeta_3 & \zeta_2+\zeta_4 \\ \zeta_2+\zeta_4 & \zeta_1-\zeta_3 \end{pmatrix} = \begin{pmatrix} \xi_1+\xi_3 & \xi_2+\xi_4 \\ \xi_2-\xi_4 & \xi_1-\xi_3 \end{pmatrix} + i \begin{pmatrix} \eta_1+\eta_3 & \eta_2+\eta_4 \\ \eta_2+\eta_4 & \eta_1-\eta_3 \end{pmatrix} \tag{5}$$

Thus, WAL invariants are as follows:

$$I_1 = (\xi_1^{\,2} + \xi_4^{\,2})^{1/2} \text{ (m/s)}, \tag{6}$$

$$I_2 = (\eta_1^{\,2} + \eta_4^{\,2})^{1/2} \text{ (m/s)}, \tag{7}$$

$$I_3 = \frac{(\xi_2^{\,2} + \xi_3^{\,2})^{1/2}}{I_1}, \tag{8}$$

$$I_4 = \frac{(\eta_2^{\,2} + \eta_3^{\,2})^{1/2}}{I_2}, \tag{9}$$

$$I_5 = \frac{\xi_4\eta_1 + \xi_1\eta_4^{\,2}}{I_1 I_2}, \tag{10}$$

$$I_6 = \frac{\xi_4\eta_1 - \xi_1\eta_4}{I_1 I_2} = d_{41}, \tag{11}$$

$$I_7 = (d_{41} - d_{23})/Q. \tag{12}$$

d_{ij} and Q parameters are dependent on ξ_i, η_i variants and the other invariants identified above and are defines as such:

$$d_{ij} = \frac{\xi_i \eta_j - \xi_j \eta_i}{I_1 I_2}, \text{ (i=1,…,4 ve j=1,…,4)} \quad (13)$$

$$Q = \left[\left(d_{12} - d_{34} \right)^2 + \left(d_{13} + d_{24} \right)^2 \right]^{1/2} \quad (14)$$

I_1 and I_2 invariants are used for finding the resistivity and phase of a 1D place:

$$\rho_{1D} = \mu_0 \frac{(I_1^2 + I_2^2)}{\omega}, \quad (15)$$

$$\varphi_{1D} = \arctan(\frac{I_2}{I_1}) \quad (16)$$

The requirements of I_3 I_4 I_5 I_6 I_7 and Q invariants necessary for the detection of galvanic distortion and dimensionality (Weaver *et al.*, 2000) are given in Table 1.

Table 1 WAL invariants and dimensional criteria (Weaver et al., 2000)

Situation	I_3-I_7 ve Q values	Dimensionality
1	$I_3 = I_4 = I_5 = I_6 = 0$ $I_1 = (\xi_1^2 + \xi_2^2)^{1/2}$ $I_2 = (\eta_1^2 + \eta_2^2)^{1/2}$	1D, Where *Mxx* and *Myy* are equal to zero and *Mxy* = -*Myx*, there is one real virtual value and one real value for a period. Resistivity and phase; $\rho_{1D} = \mu_0 \frac{(I_1^2 + I_2^2)}{\omega}$, $\varphi_{1D} = \arctan(\frac{I_2}{I_1})$, except I_1 and I_2, all other constants (I_3 - I_7 ve Q) are equal to zero.
2	$I_3 \neq 0 ve ya I_4 \neq 0$; $I_5 = I_6 = 0$; $I_7 = 0 ve ya Q = 0$ $(\xi_4 \neq 0 ve \eta_4 \neq 0)$	2D, If Q is too small, $(I_3 \approx I_4) I_7$ can be regarded as zero even though it is undefined. The strike angle is $\tan 2\theta' = -\frac{\xi_3}{\xi_2} = -\frac{\eta_3}{\eta_2}$.
3	$I_3 \neq 0 ve ya I_4 \neq 0$; $I_5 \neq 0; I_6 = 0$; $I_7 = 0$	3D/2D2D, Situation affected by galvanic distortion (only twist) strike angle; $\tan 2\theta' = -\frac{d_{12} - d_{34}}{d_{13} + d_{24}}$.
4	$I_3 \neq 0 ve ya I_4 \neq 0$; $I_5 \neq 0; I_6 \neq 0$; $I_7 = 0$	3D/2D, The overall state of the galvanic distortion on a 2D structure is strike angle; $\tan 2\theta' = -\frac{d_{12} - d_{34}}{d_{13} + d_{24}}$
5	$I_7 \neq 0$	3D, (affected or unaffected by galvanic distortion)
6	$I_3 \neq 0 ve ya I_4 \neq 0$; $I_5 = I_6 = 0$; $Q = 0 ve ya I_7 = 0$ $(\xi_4 = 0 ve \eta_4 = 0)$	3D/1D2D, (Diagonal) 1D or 2D structures with galvanic distortion strike angle; $\tan(2\theta') = \frac{\xi_2}{\xi_3} = \frac{\eta_2}{\eta_3}$
7	$I_3 \neq 0 ve ya I_4 \neq 0$; $I_5 \neq 0; I_6 = 0$; $Q = 0$	3D/1D2D, Galvanic distortion exists in equal-phase 1D or 2D environments at polarities electrical area and magnetic area. These two conditions are indistinguishable, but in the second (distortion in 2D) it is not possible to determine strike direction. $I_3 = I_4$ and I_5 is non-zero, and Q is zero and Q=0, $I_3 = I_4$, I_7 is undefined.

5. DIMENSION OF THE REGION BETWEEN ZONGULDAK AND AKSEHIR

I_1 , I_2 , I_3 , I_4 , I_5 , I_6 , I_7 and Q values, strike directions and distortion parameters of the WAL invariants developed by Weaver et al. (2000) were calculated at 80 frequency for each measurement. Maps that display the distribution of WAL invariant values in different locations and different periods in the profiles were created. In addition to these, the dimensionality types in the 174 stations along profile 1 and profile 2 for different periods were mapped. Thus, contour maps showing the distribution of the WAL invariants in different depths were formed and analyzed. Lastly, pseudo-sections were created using WAL invariants, vertical axis being the period and horizontal axis being the distance.

In order to show the change in the values of WAL invariants acquired in the logarithmic period bands for MT data and each measurement; and to show the values used in dimensionality, KBA is contoured as a map. The figures below show the contour maps of the WAL invariants in fixed periods such as T=0.01, 0.1, 1, 10, 100, 1000s.

Fig. 3 shows the change of I_3 for logarithmic periods. According to this figure, I_3 is usually low through both profiles in T=0.01s and T=0.1s. While I_3 has a high value in T=1s map in the northern section of the 1st profile and the middle of the 2nd profile, it has low values in other parts. I_3 usually has high values in T=1s, T=10s and T=100s. I_3 value is again usually high in T=1000s in the northern section of the 1st profile and middle of the 2nd profile, while it is low in other parts.

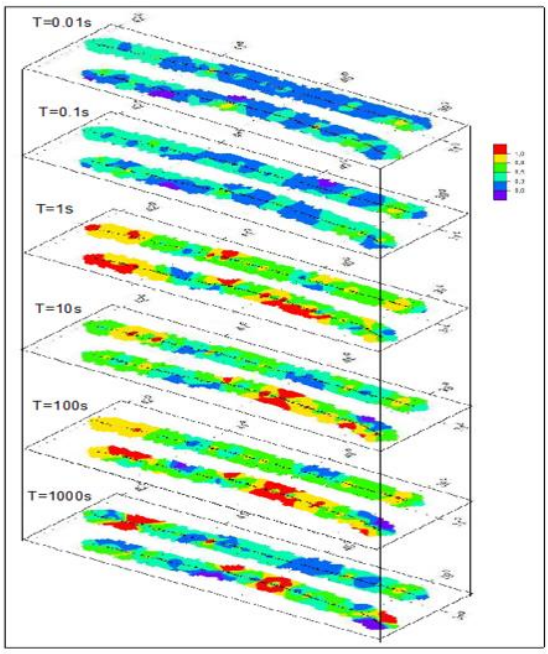

Fig. 3. Contour maps of the WAL constant I_3 at T = 0.01, T = 0.1, T = 1, T = 10, T = 100 and T = 1000 periods.

Fig. 4 shows the changes of I_4 values in the maps prepared for the logarithmic periods. I_4 values are high in the middle section of the 2nd profile for the periods

T=0.01s, T=1s and T=10s. In these periods, values are usually low in the 1st profile. I_4 values are low in the T=0.1s in both profiles. While I_4 values are usually high throughout the 2nd profile for T=1000s, they drop in the northern section of the 1st profile.

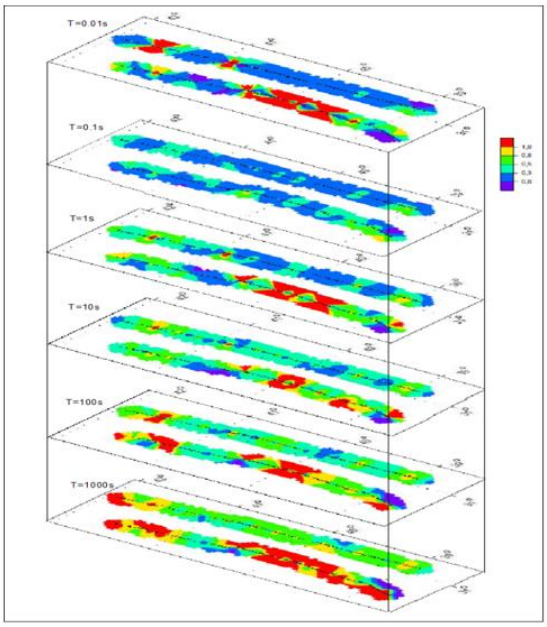

Fig. 4. Contour maps of the WAL constant I_4 at T = 0.01, T = 0.1, T = 1, T = 10, T = 100 and T =1000.

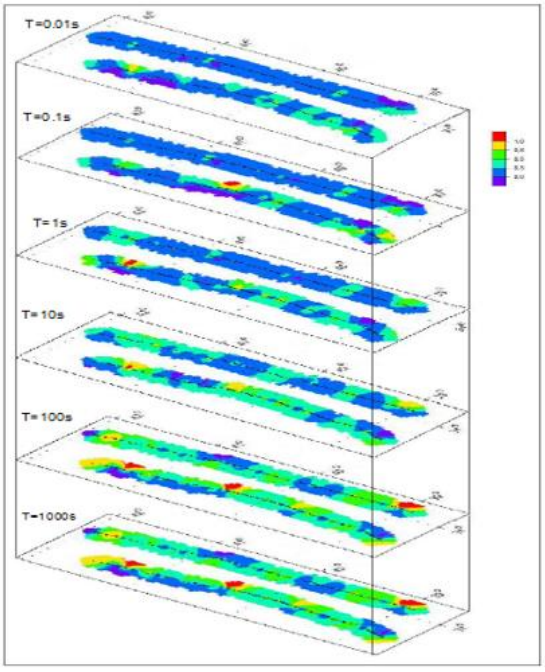

Fig. 5. Contour maps of the WAL constant I_5 at T = 0.01, T = 0.1, T = 1, T = 10, T = 100 and T =1000.

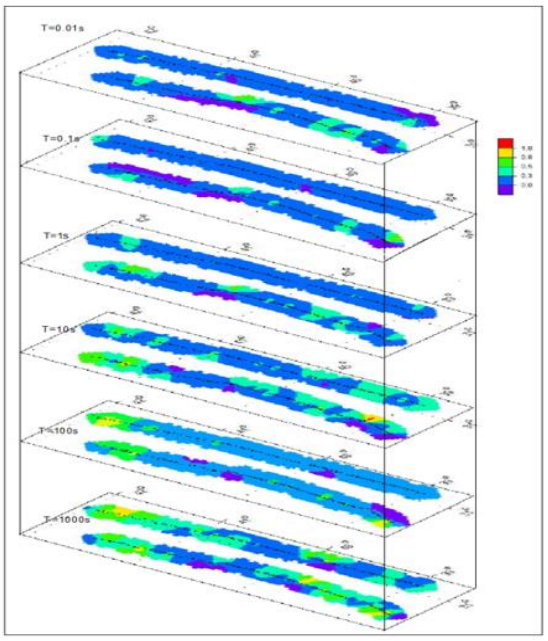

Fig. 6. Contour maps of the WAL constant I_6 at T = 0.01, T = 0.1, T = 1, T = 10, T = 100 and T =1000.

When the changes in I5 in the stated fixed periods (Fig. 5) are analyzed, it is observed that the values in the first three maps are usually high and gradually increases in the other maps. The changes in I6 throughout the 1st Profile and the 2nd Profile are shown in Fig. 6. According to the figure shown, I6 values in T=0.01s, T=0.1s and T=1s are usually low throughout both profiles. However, in T=10s and T=100s maps, I6 value increases in the north of the 1st and 2nd Profiles. While I6 value also increases in both the northern and southern sections of the 1st and 2nd Profiles, it is usually low in the middle section.

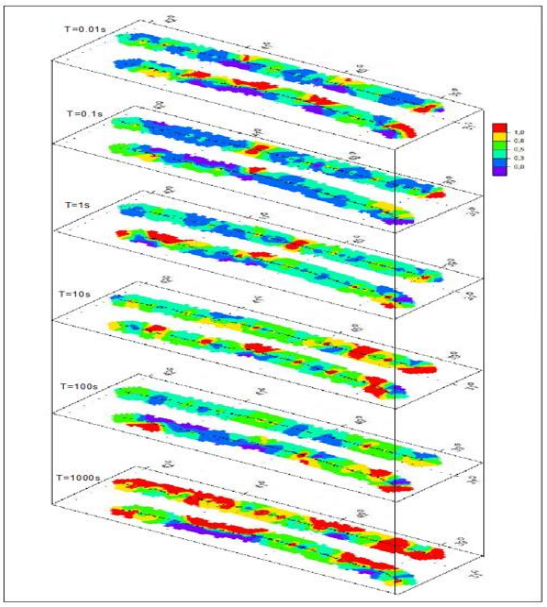

Fig. 7. Contour maps of the WAL constant I_7 at T = 0.01, T = 0.1, T = 1, T = 10, T = 100 and T = 1000 periods.

Changes in the value in specific fixed periods throughout the 1st Profile and the 2nd Profile are shown in Fig. 7. Changes are observed in I7 values in T=0.01s and T=0.1s throughout both profiles. While I7 value is observed to be usually high in T=1s in the south of the 1st and the 2nd Profile decreasing towards the north, it is also observed that the I7 value increases again in the northern section of the 2nd Profile. I7 values are usually high in T=10s, T=100s and T=1000s but I7 values are low in the northern section of the 2nd Profile in T=100s.

The changes in *Q* throughout the 1st Profile and the 2nd Profile are shown in Fig. 8. According to the figure, there are high values in the northern section of the 1st Profile while there are low values in the other sections. The *Q* values are high in the middle section of the 2nd Profile while they are low in the other sections. *Q* values are low throughout the 1st Profile in T=0.1. The values are also low in the northern section of the 2nd Profile but high in the other sections. The distribution in T=1s is similar to that in T=0.01s. In T=10s, there are usually low values in the 1st Profile while high values are observed in the northern section of the 2nd Profile. Values are usually low in the 1st Profile in T=100s and T=1000s. While the *Q* values are high in the northern section of the 2nd Profile and in the inner sections in T=100s, they are low in the other sections. *Q* values are high throughout the 2nd Profile in T=1000s.

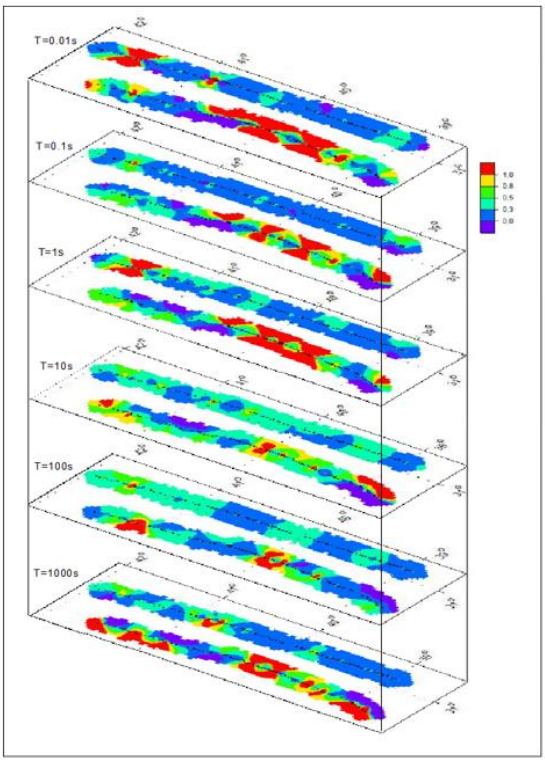

Fig. 8. Contour maps of the WAL constant *Q* for periods T = 0.01, T = 0.1, T = 1, T = 10, T = 100 and T = 1000.

6. DIMENSIONALITY ANALYSIS OF STUDY AREA

In this chapter, dimensionality analysis was performed for each point in all periods similar to the study by Marti (2004). $\tau = 0.15$ and $\tau_Q = 0.1$ threshold values tested and applied by Marti et al. (2004) for WAL invariants were used for determining the dimensionality. Because, WAL invariants can never be equal to zero (Weaver et al., 2000). Dimensionality maps were obtained by grouping the results on logarithmic period bands. The average strike directions for 2D and 3D/2D regions were drawn along with their standard deviations. Strike directions were scaled inversely proportional to error values. In short periods, there is complexity in dimensionality due to the local shallow materials that cause distortion in the measured data. Dimensionality is less complex in the long periods compared to the short ones.

WAL criteria were taken into consideration in this calculation. The reason for WAL invariants to be used instead of other methods is that it uses all the information obtained from the MT tensor and identifies dimensionality accordingly.

It is observed in Fig. 9 that the 1st band (0.001-0.01) is usually represented by 3-Dimensionality and 2-Dimensionality. When analyzed in detail, it is observed that there are 3D /2D and 2D structures in NE-SW strike directions in the first ten MT stations around Turgut (Konya) located on the Tauride-Anatolide Block in the south. However, the area between the points1010-1020, around Çeltik, is 1D. Dimensionality changes between the Tauride-Anatolide Block and the Sakarya Continent at the İzmir-Ankara Suture Zone and displays 3/2/1 dimensionality. There are 2D structures with NE-SW strike directions on points 1035 and 1036. 3D/2D, 3D, 1D structures are observed moving towards north. Some NE-SW trending 2D structures are observed near the Çeltikçi fault zone in parallel to the fault zone. The southwest of Kıbrıscık is represented by 1 Dimensionality. Moving towards north, the dimensionality becomes complex again near Bolu and 1D, 3D, NE-SW trending 3D/2D and 2D structures are noticed. This section corresponds to the Intra-Pontide Suture located between the Sakarya Continent and İstanbul Zone. Although there are some 1D, N-S trending 3D/2D structures are observed in some parts around Devrek and Zonguldak located at the northernmost section of the 1st Profile, there are also some 3D structures in some parts.

When the second profile in Fig. 9 is analyzed it is observed that most of the points located on the Tauride-Anatolide block, the southernmost section on the map, are 3D. On the inner section of the map, on points 2028-2036, the dimensionality is 1D and a change is observed around the Eskişehir fault zone. In this region there are 3D, 3D/2D/1D structures are located and there are also some 2D and 3D/2D structures with different strike directions considered to be due to other curves and faults of different trends. Beylikova vicinity and the west of Mihalıççık are represented by 1 Dimensionality. There are some 3D structures between points 2050-2058. In the southwest of Nallıhan, dimensionality is 3D, 3D/2D/1D, 1D and there are E-W trending 3D/2D structures. Considering that the dimensionality changes significantly in this region, it could be said that this region is similar to the İzmir-Ankara suture zone.

Between the points 2062-2066, there are usually NE-SW trending 3D/2D structures with different angles. There are 3D, 1D and NE-SW trending 2D structures near the North Anatolian Fault zone. Moving towards the north, 3-Dimensionality is more dominant between

the Karadere Kaynaşlı Mengen Sub Fault Zone and Akçakoca.

In Fig. 10, results of the dimensionality analysis obtained from the WAL invariants on T=0.01-0.1s period band for measurement points 1001-1084 from south to north throughout the 1st Profile. When this figure is analyzed, 2D structures are observed between points 1001-1008 at the southernmost section of the profile. These structures also display strike directions of N19E and N46E. In the section between points 1009 and 1020 there are some 2D and 1D structures with strike directions of N46E and N82E. The structures between points 1020-1025 are 3D. Most of the structures between points 1025-1037 are 1D. While there are mostly 3D structures between stations 1038-1045, there are also some 3D/2D structures with N65E and N26E strike directions. The dimensionality between points 1046-1065 is usually 3D/2D. The strike directions of these structures range between N32E and N83E from south to north. The structures between points 1065-1072 are 1D, 3D/2D and 3D. The dimensionality of points 1072, 1073 and 1074 is 2D and the strike direction of these structures is N71E. There are usually 3D structures between points 1075-1084 located at the northernmost section of the profile and there are some 3D/2D/1D structures at some points.

Fig. 10 shows the dimensionality analysis results obtained from WAL parameters on the T=0.01-0.1 period band for measurement points 2001-2090 throughout the 2nd Profile from south to north. According to this figure, there are 3D structures affected by the galvanic distortion in places between measurement points 2001-2008 at the southernmost point of the profile. The dimensionality between points 2008-2014 is 3D/2D/1D and 2D. The places between points 2014-2029 are generally 3-Dimensional; however, there are also 3D/2D structures with N81E strike direction near the measurement point 2042. The dimensionality between points 2045-2050 is 1D. It is observed that there are 3D structures; 2D structures with N54E strike direction; 3D/2D structures with N20E strike direction and 3D/2D/1D structures between points 2050-2060. In the region where points 2060-2076 are located there are 3D/2D structures with N25E strike direction; 2D structures with N71E strike direction and 1D structures in some parts; however, the region is mostly represented by 3D structures. Dimensionality of all points on the İstanbul zone, which is located at the northernmost section of the 2nd Profile, is 3D.

Fig. 11 shows the dimensionality analysis results obtained from WAL parameters on T=0.1-1s period band for measurement points 1001-1084 throughout the 1st Profile, from south to north. According to this figure, the dimensionality between the first points 1001-1012 on the Tauride-Anatolide Block located at the southern most section of the 1st Profile on the 3rd band is 3D. While the dimensionality between points 1012-1020 is mainly 1D, there are also 2D structures with N78E strike direction between points 1013 and 1014. The dimensionality between points 1020-1027 is generally 3D. There are 1D and 3D structures between points 1027 and 1040. The dimensionality of the places between points 1040-1066 is complex with 1D structures, 2D structures with N60E strike angle and 3D/2D, 3D, 3D/2D/1D structures with N50E strike direction. In addition, there are generally 3D/2D structures with N55E strike direction between points 1066-1073. However, point 1072 is 2D and its strike direction is N73E. The dimensionality between points 1073-1084 located at the northernmost section of the profile on the İstanbul Zone is 3D.

Fig. 11 shows the dimensionality analysis results obtained from WAL parameters on T=0.1-1s period band for measurement points 2001-2090 throughout the 2nd Profile, from south to north. According to this figure, on the 3rd band there are usually 3D structures between points 2001-2012 located at the southernmost section of the 2nd Profile and there are some 2D and 3D/2D structures, as well. The dimensionality between points 2012-2039 is 3D. There are 3D/2D structures with N35E strike direction at points 2039, 2040 and 2041. Points 2042, 2043, 2044 are 3D and points 2045, 2046 and 2047 are 1D. There are generally 3D structures between points 2047-2065. There are 3D/2D structures with N60E strike direction between points 2065-2070. There are 3D structures at 2070-2090 stations.

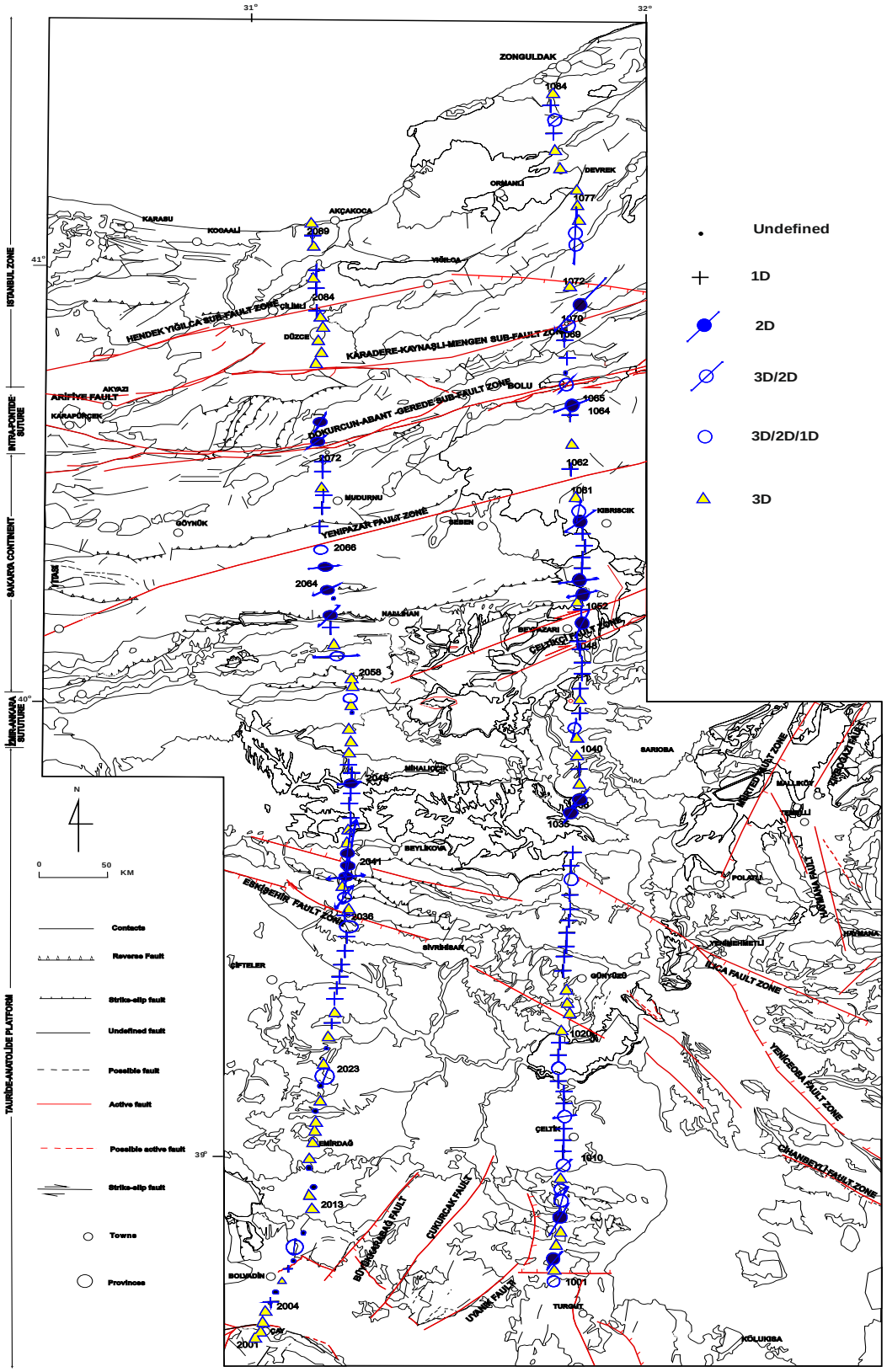

Fig. 9. Shows the KBA dimensionality analysis results on T=0.001s-0.01s band. Arrows show the strike direction. 3D/2D twist and 3D/2D are drawn as a single incident (3D/2D). Strike directions were scaled inversely proportional to error values. Certain signes are used for the existence of certain structures.

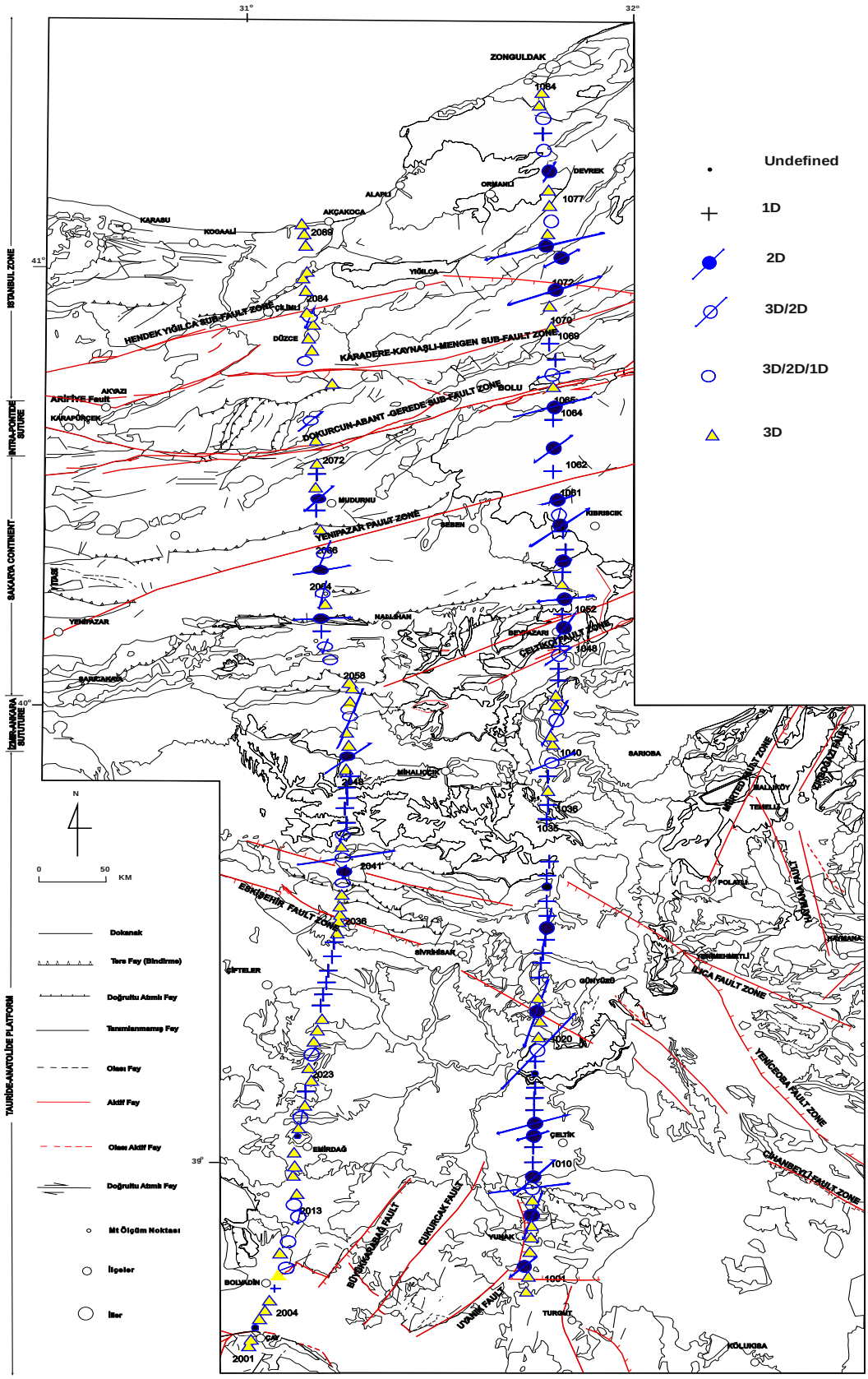

Fig.10. Shows the KBA dimensionality analysis results on T=0.0s-0.01s band. Arrows show the strike direction. 3D/2D twist and 3D/2D are drawn as a single incident (3D/2D). Strike directions were scaled inversely proportional to error values. Certain signes are used for the existence of certain structures.

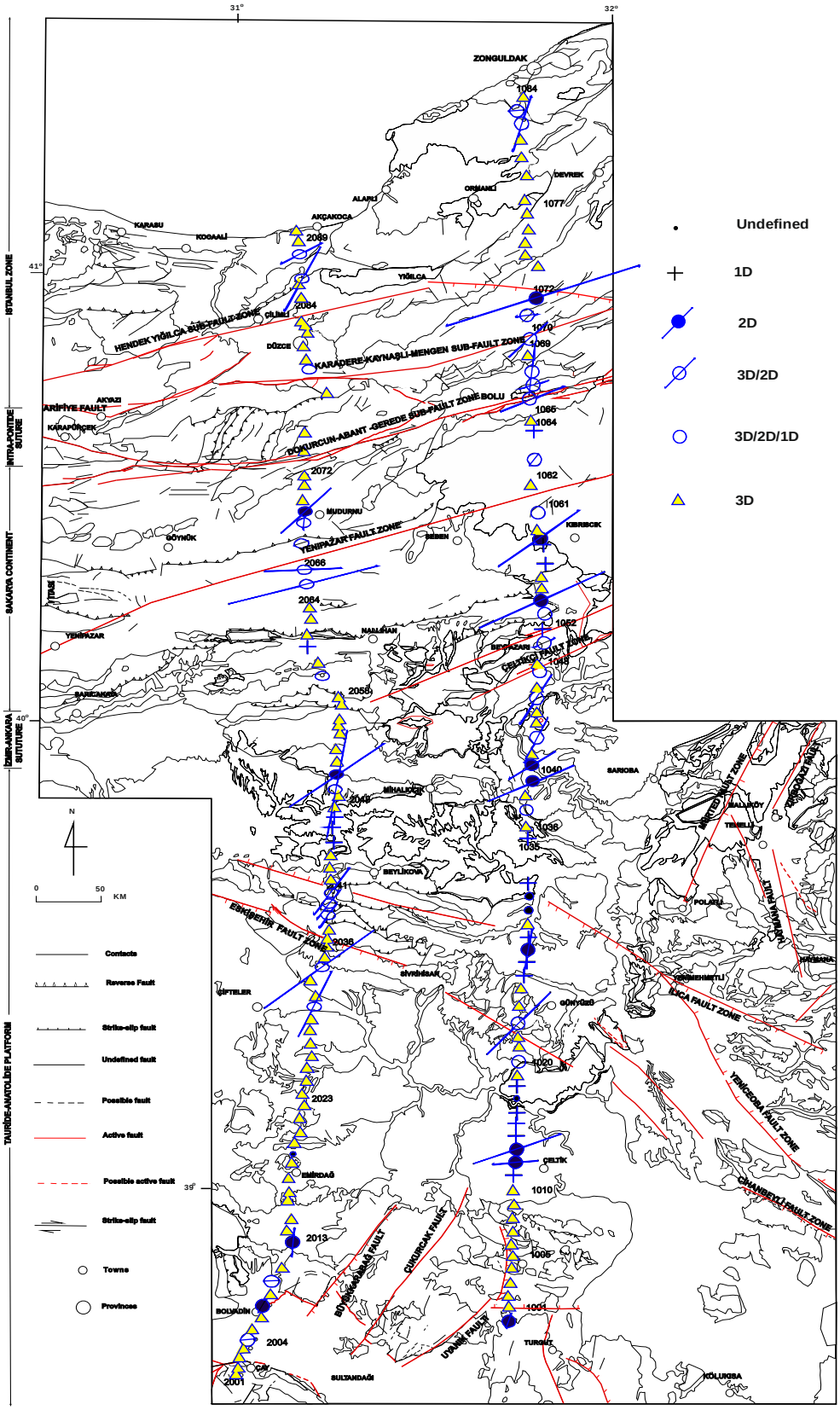

Fig. 11. Shows the KBA dimensionality analysis results on T=0.0s-0.01s band. Arrows show the strike direction. 3D/2D twist and 3D/2D are drawn as a single incident (3D/2D). Strike directions were scaled inversely proportional to error values. Certain signes are used for the existence of certain structures.

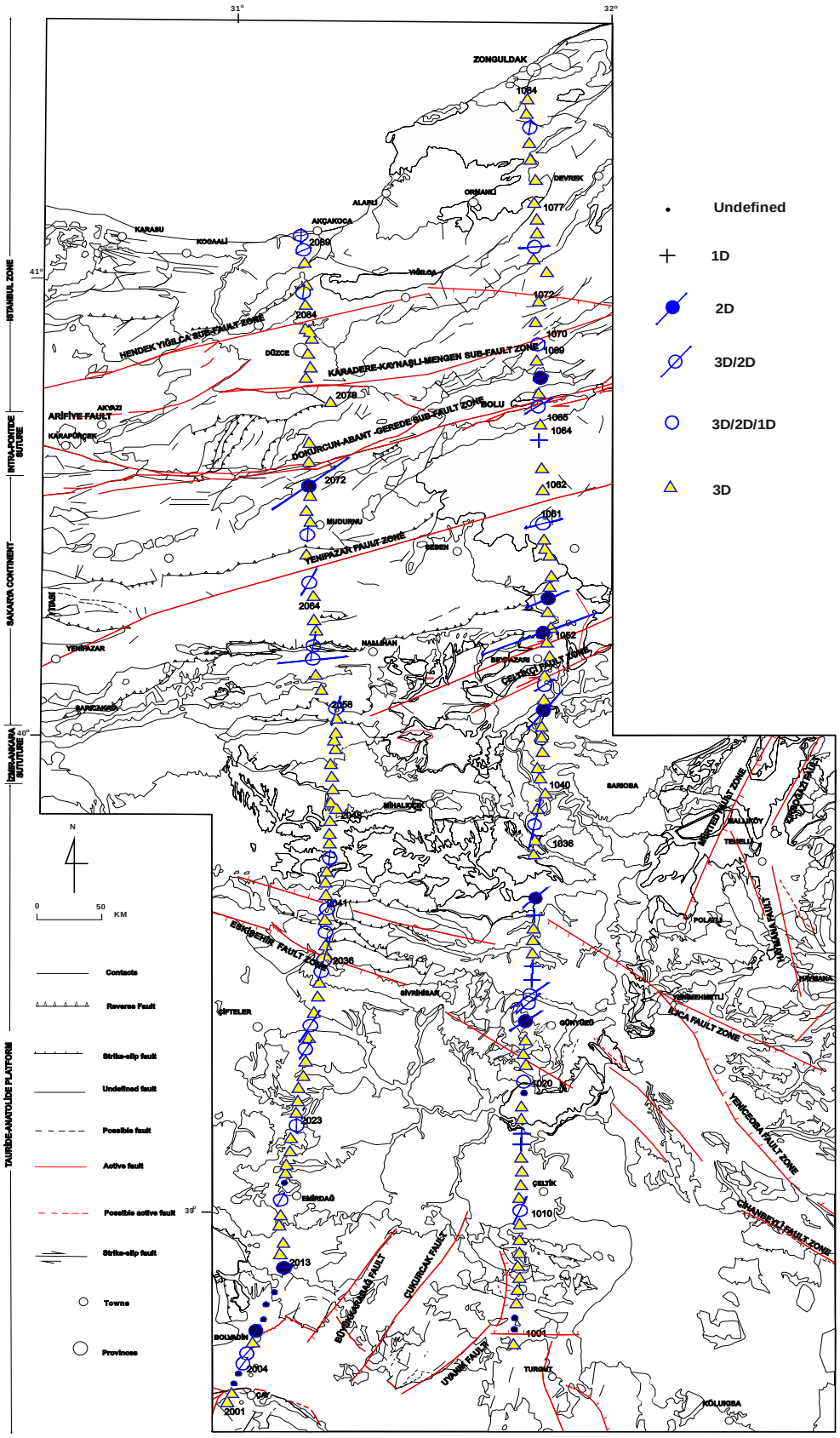

Fig. 12. Shows the KBA dimensionality analysis results on T=0.0s-0.01s band. Arrows show the strike direction. 3D/2D twist and 3D/2D are drawn as a single incident (3D/2D). Strike directions were scaled inversely proportional to error values. Certain signes are used for the existence of certain structures.

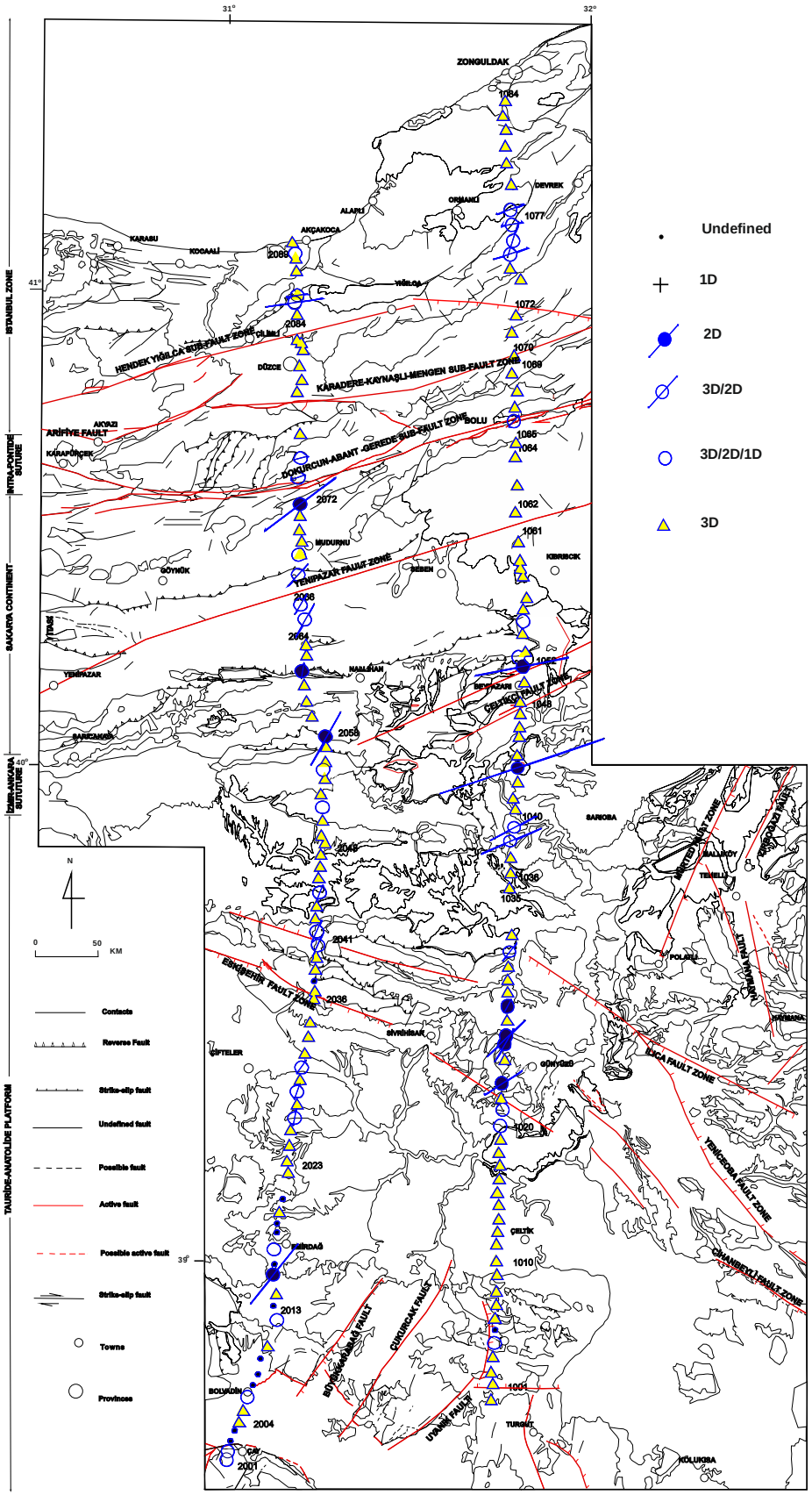

Fig. 13. Shows the KBA dimensionality analysis results on T=0.0s-0.01s band. Arrows show the strike direction. 3D/2D twist and 3D/2D are drawn as a single incident (3D/2D). Strike directions were scaled inversely proportional to error values. Certain signes are used for the existence of certain structures.

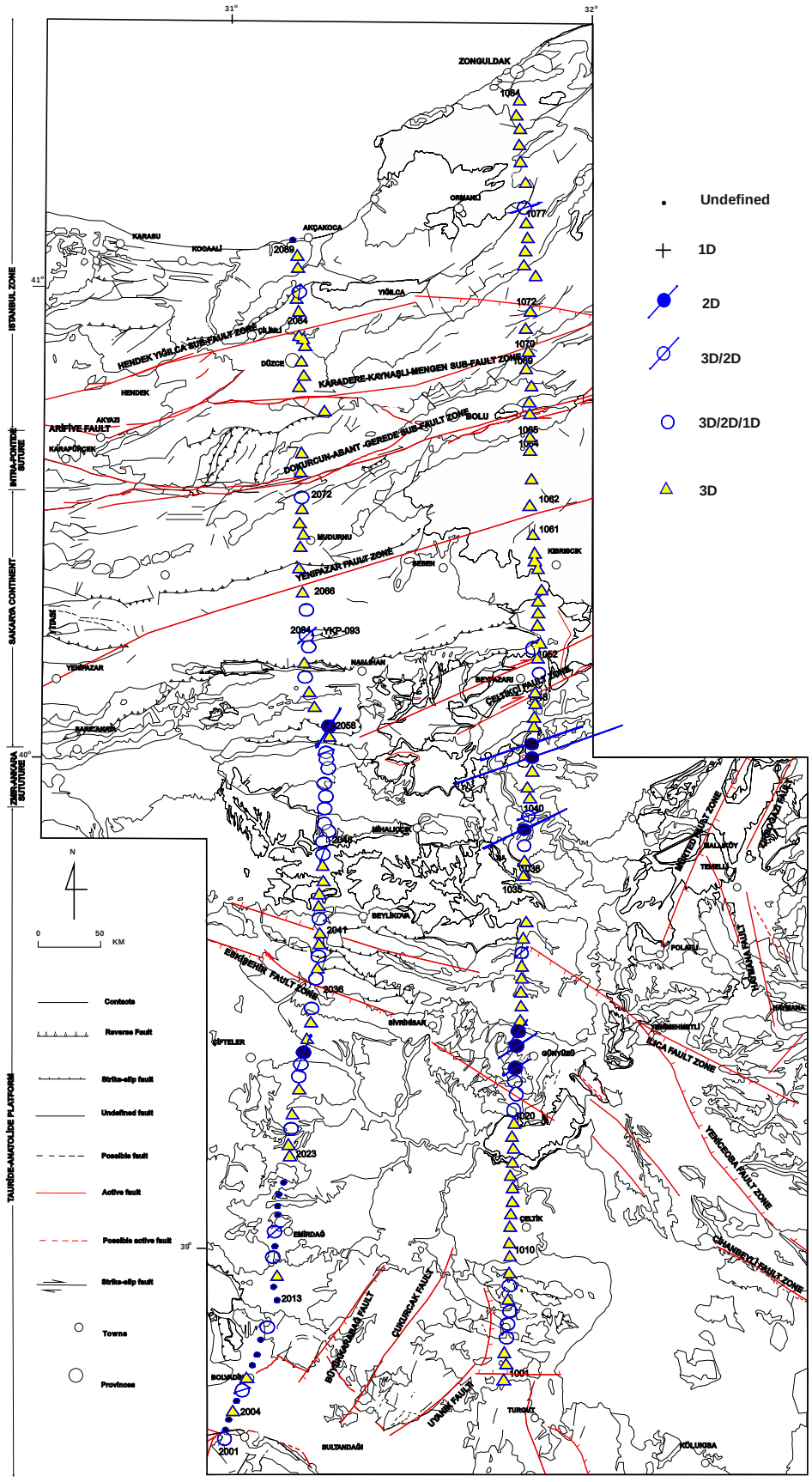

Fig. 14. Shows the KBA dimensionality analysis results on T=0.0s-0.01s band. Arrows show the strike direction. 3D/2D twist and 3D/2D are drawn as a single incident (3D/2D). Strike directions were scaled inversely proportional to error values. Certain signes are used for the existence of certain structures.

Fig. 12 shows the dimensionality analysis results obtained from WAL parameters on T=1-10s period band for measurement points 1001-1084 throughout the 1st Profile, from south to north. According to the figure, the most of the 1st Profile is 3D on the 4th band. Moving towards the north, some 2D structures with N60E strike angle and 3D/2D structures with N56E strike angle are also observed among these 3D structures.

Fig. 12 shows the dimensionality analysis results obtained from WAL parameters on T=1-10s period band for measurement points 2001-2090 throughout the 2nd Profile, from south to north. According to the figure, the most of the 2nd Profile is 3D on the 4th band.

Fig. 13 shows the dimensionality analysis results obtained from WAL parameters on T=10-100s period band throughout the 1st Profile, from south to north. According to this figure, there are 3D structures between points 1001-1023. The area between points 1023-1029 is represented by 2D structures with N46E strike angle and the area between points 1029-1075 is generally represented by 3-dimensionality and there are also a small number of 3D/2D structures with N66E strike. The dimensionality of points 1075-1078 is 3D/2D and the strike angle is N61E. The areas between points 1078-1084 located at the northernmost section of the 1st profile is 3D.

Fig. 13 shows the dimensionality analysis results obtained from WAL parameters on T=100-1000s period band for measurement points 2002-2090 throughout the 2nd profile, from south to north. According to this figure, the dimensionality at the first 21 points at the southernmost section of the 2nd profile is 3D and 3D/2D/1D. However, dimensionality could not be determined at most of the measurement points. While it is 3D between points 2021-2027, there are 3D structures and 3D/2D structures with N24E strike angle between points 2027-2031. The dimensionality between points 2031-2039 is 3D. Between points 2041-2046 there are 3D/2D and 3D structures with N24E strike angle. The dimensionality between points 2046-2065 is generally 3D. Among these 3D structures, there are also some 2D structures with N21E strike angle. The dimensionality at points 2065, 2066, 2067 is 3D/2D and the strike angle is N35E. The dimensionality between points 2068-2071 is 3D. The dimensionality at points 2072, 2074, 2075 is 3D/2D and 2D and the strike angle is N68E. The other points up to 2090 located at the northernmost section are mainly 3D.

Fig. 14 shows the dimensionality analysis results obtained from WAL parameters on T=100-1000s period band for measurement points 1001-1084 throughout the 1st profile, from south to north. According to this figure, there are 3D structures at the first 3 points of the 1st profile. Between points 1004-1009 there are some undistinguishable structures that could either be 3D/2D or 3D/1D. There are 3D structures between points 1009-1021. There are 2D structures with N51E strike and 3D/2D/1D structures between points 1021-1027. The structures located between points 1027-1039 are 3D. At points 1039, 1040 and 1044, 1045 there are 3D/2D structures with 70° strike angle and NE direction and 2D structures. The dimensionality of all other points up to 1084 at the northernmost section is 3D.

Fig. 14 shows the dimensionality analysis results obtained from WAL parameters on T=100-1000s period band for measurement points 2001-2090 throughout the 2nd profile, from south to north. According to this map, dimensionality could not be determined at some points in the south of the 2nd profile. It could only be determined at some points and usually there are some 2D structures and 3D structures observed with high error rates. The structures between points 2023-2048 are usually 3D and there are also 3D/2D/1D structures at some areas. The dimensionality between points 2048-2056 is 3D/2D/1D and between points 2056-2066 it ranges from 3D to 3D/2D/1D. At all other points to the north of 2066, mainly 3-dimensionality is observed.

7. DIMENSIONAL SECTIONS

WAL invariants for 80 periods were calculated based on the MT data from 174 stations throughout 2 profiles from the region between Zonguldak and Akşehir. Dimensionality states were obtained in accordance with WAL criteria on 80 periods for the 174 MT data and the data were contoured on Win G link program as vertical axis being the period and horizontal axis being the distance and dimensionality sections were obtained accordingly. Fig. 15 shows the changes in dimensionality throughout the 1stprofile and the 2nd profile according to the period and the distance.

In Fig. 15, the dimensionality between 0.01-1s periods in the 1st profile is represented by 2D and 1D. 3D and 3D/2D dimensionality is mainly observed between periods 1-100s. The dimensionality between periods 100-10000s is 1D and 2D.

The dimensionality distribution in the 2nd profile is similar to that of the 1st profile. The dimensionality between periods 0.01-1s is represented by 2D and 1D. 3D and 3D/2D dimensionality is mainly observed between periods 1-100s. The dimensionality between periods 100-10000s is 1D and 2D.

Looking at the sections given below, it is possible to say that the sections in both profiles can be vertically divided into three sections. This could be interpreted as the upper crust, lower crust and upper mantle sorting, respectively, for the geoelectric section of the YKP profile suggested by Kaya (2010) (Fig. 16 a)).

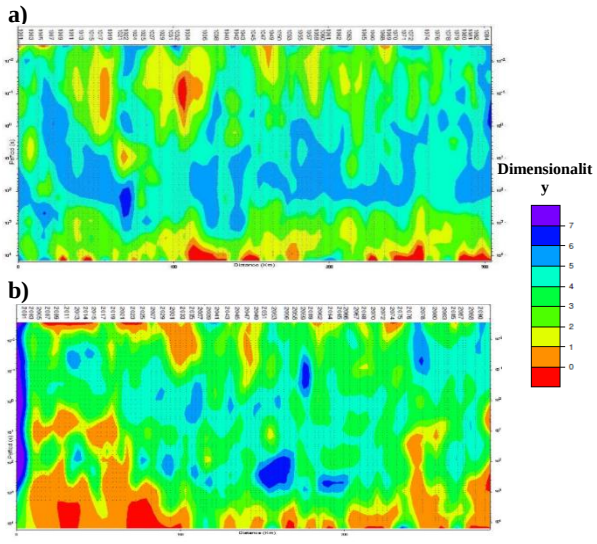

Fig. 15. Dimensional sections prepared according to WAL constants criteria a) Profile 1, b) Profile 2

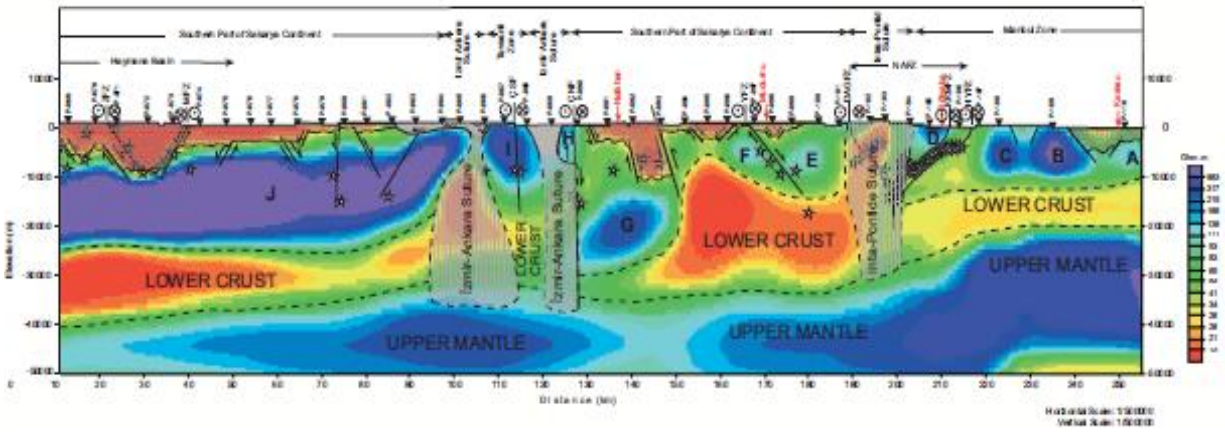

Fig. 16. a) The 2D resistivity model obtained as a result of inverting the MT data measured along a line close to the study area which obtained from the YKP points located in Fig. 1 (Kaya, 2010).

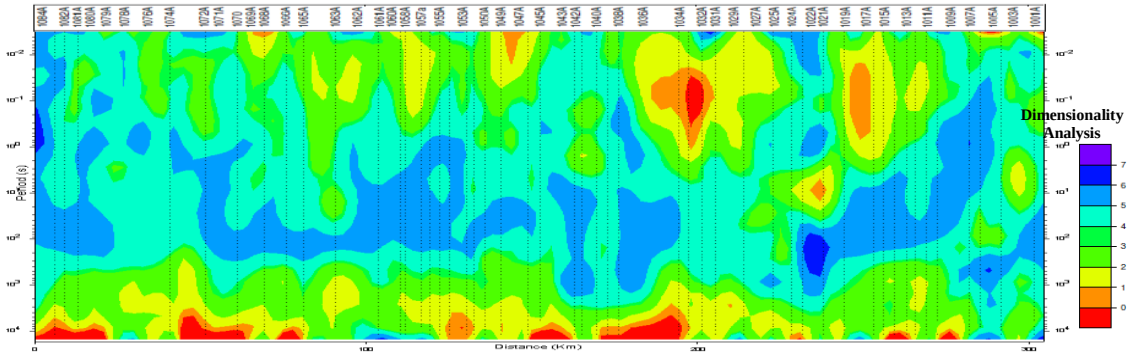

Fig. 16. b) Dimensional cross-section prepared according to WAL constants criteria along profile

8. CONCLUSIONS

As a result of the dimensionality analysis obtained from the KBA's MT data, 2D and 3D structures were revealed. The areas that were detected as 3D in 2D evaluation of the MT data should be interpreted more carefully.

The distinction between the upper crust and the lower crust can be observed more clearly when the dimensionality sections prepared in accordance with the WAL invariants criteria are analyzed (Fig. 16a and Fig. 16b).

According to the dimensionality maps;

- It was observed that the dimensionality was complex in short periods due to conductive heterogeneous materials close to the surface and 3D structures were more predominant in long periods.
- Moreover, it was observed that the dimensionality was more complex in areas near the suture zones according to the dimensionality analysis results.
- The strike directions of the structures near the North Anatolian Fault were generally N-NE.

These results show that dimensionality can be correlated to the geo-electric structure and geology. This should definitely be used in the evaluation of magnetotelluric measurement results.

ACKNOWLEDGEMENTS

This work, which includes a part of the graduate thesis (Kaçmaz, 2009) of Fahriye Akar, was supported by Cumhuriyet University Scientific Research Projects (CÜBAP, under grant no: M-350) and Scientific and Technological Research Council of Turkey (TUBITAK, under grant no: 105G145).

REFERENCES

Bahr, K., 1988, Interpretation of the magnetotellüric impedance tensor: regional induction and local tellüric distorsion. J.Geophys., 62, 119-127

Bahr, K., 1991. Geological noise in magnetotellüric data : a classification of distortion types, Phys. Earth planet. Inter., 66, 24-38.

Berdichevsky, M. N. and Dmitriev, V. I., 1976, Basic principles of interpretation of magnetotellüric sounding curves, In: Geoelectric and Geothermal studies, Ed.: Adam, A. Budapest, Akademai Kiado, 165-221.

Caldwell, T.G., Bibby, H.M., Brown, C., 2004. The Magnetotelluric Phase Tensor, Geophys. J. Int, 158,457-469.

Fischer, G. And Masero, W., 1994. Rotational properties of the magnetotelluric impedance tensor, the example of

the Araguainha impact crater, Brazil, Geophys. J. Int., 119, 548-560.

Ingham, M.R., 1988. The use of invariant impedance in magnetotelluric interpretation, Geophys. J., 92, 165-169.

Kaçmaz, F. 2009. Magnetotelluric Investigation of Zonguldak-Aksehir Region Crustal Structure And Dimensionality Analysis, Graduate Thesis, 83 pp., Institute of Science, Cumhuriyet University, Turkey.

Kaya, C., 2010. Deep Crustal Structure of Northwestern Part of Turkey, Tectonophysics, 489, 227-239.

Lilley, F.E.M., 1976, Diagrams for magnetotelluric data: Geophysics, 41, 766–779.

Lilley, F.E.M., 1993a, Mohr circles in magnetotelluric interpretation (i) simple static shift; (ii) Bahr's analysis: Journal of Geomagnetism and Geoelectricity, 45, 833–839.

Lilley, F.E.M., 1993b, Three-dimensionality of the BC87 magnetotelluric data set studied using Mohr circles: Journal of Geomagnetism and Geoelectricity, 45, 1107–1113. Lilley, F.E.M., 1993c, Magnetotelluric analysis using Mohr circles: Geophysics, 58, 1498–1506.

Lilley, F.E.M., 1998a, Magnetotelluric tensor decomposition: Part I, Theory for a basic procedure: Geophysics, 63, 1885–1897.

Lilley, F.E.M., 1998b, Magnetotelluric tensor decomposition: Part II, Examples of a basic procedure: Geophysics, 63, 1898–1907.

Okay, A.I., 1989. Tectonic units and sutures in the Pontides, northern Turkey. In: A.M.C. Şengör, (Ed.), Tectonic evolution of the Tethyan region. Kluwer Academic Publications, Dordrecht: 109–115.

Okay, A.I. and Mostler, H., 1994. Carboniferous and Permian radiolarite blocks from the Karakaya Complex in northwest Turkey. Turk. J. Earth Sc., 3: 23-28.

Okay, A.I., Tüysüz, O., 1999. Tethyan sutures of northern Turkey. In "The Mediterranean Basins: Tertiary extension within the Alpine orogen" (eds. B. Durand, L. Jolivet, F. Horváth and M. Séranne), Geological Society, London, Special Publication 156, 475–515.[3]

Ranganayaki, R. P., 1984, An interpretativite analysis of magnetotelluric data:Geophysics, 49, 1730-1748.

Park, S. W. and Livelybrooks, D.W., 1989. Quantative interpretation of rotationally invariant parameters in magnetotellürics, Geophysics, 54, 1483-1490.

Romo, J. M., Gomez-Trevino, E. and Esparza, F. J., 1999. An invariant representation of the magnetic transfer function in magnetotellürics, Geophysics, 64, 1418-1428.
Smith, J. T., 1995. Understanding telluric distortion matrices, Geophys. J. Int., 122, 219-226.

Swift, C. M., 1967. A magnetotelluric investigation of an electrical conductivity anomaly in the southwestern United States, Ph.D. thesis, Massachusetts Institute of Technology, Cambridge, MA.

Szarka, L. and Menveille, M., 1997. Analysis of rotational invariantsof the magnetotellüric impedance tensor, Geophys. J. Int., 129, 133-142.